Commun Nonlinear Sci Numer Simulat 18 (2013) 2129–2141

Contents lists available at SciVerse ScienceDirect

Commun Nonlinear Sci Numer Simulat

journal homepage: www.elsevier.com/locate/cnsns

A spectral element approach for the stability analysis of time-periodic delay equations with multiple delays

Firas A. Khasawneh [a,*], Brian P. Mann [b]

[a] Department of Civil and Environmental Engineering, Duke University Durham, NC 27708, United States
[b] Department of Mechanical Engineering and Materials Science, Duke University Durham, NC 27708, United States

ARTICLE INFO

Article history:
Received 12 June 2012
Accepted 30 November 2012
Available online 23 December 2012

Keywords:
Delay equations
Multiple time delays
Spectral element
Stability

ABSTRACT

This paper describes a general spectral element approach to study the stability of multiple time delay systems (MTDS). We show, for the first time, how this approach can be applied to periodic MTDS where the delays and the period are incommensurate. In contrast to prior works on MTDS, the spectral element approach is applicable to both autonomous as well as non-autonomous MTDS. Both MTDS of first order or higher can be obtained and systems with or without damping can be investigated. Since the spectral element approach uses efficient interpolation and a set of well-distributed interpolation points, the size of the matrices necessary for convergence is kept small. Further, since the spectral element approach is a semi-analytical procedure, it avoids the need to use tedious time marching algorithms to explore the stability behavior of the system.

1. Introduction

The last 50 years have seen an increasing interest in the analysis of delay systems. This interest is strongly motivated by the ubiquity of physical and biological models that include delays. For example, delays are inherent to many physical systems such as machining processes and lasers [1–3]. Delays can also enter the system's equation as a modeling decision to characterize complex processes that are known to take a certain amount of time, e.g. epilepsy seizure models [4]. In addition, delayed signals have been used in efficient control schemes even when the mathematical model of the system is too complicated or unavailable [5,6].

Although delays have important applications in science and engineering, their infinite dimensional state space significantly complicates their analysis. Further, even low-order delay equations can exhibit very complicated dynamics [7]. Due to the difficulties associated with the analyical treatment of delay differential equations (DDEs), a significant number of works focus on solving DDEs numerically. The majority of these works have focused on either extending Runge–Kutta methods to DDEs or on using an implicit Radau method [8–11].

However, we are interested in the long-term dynamics, namely the stability of equilibria. For example, consider the nonlinear delay equation

$$\frac{dx}{dt} = g(x(t), x(t-\tau_1), x(t-\tau_2), \ldots, x(t-\tau_{n_\tau})), \tag{1}$$

with the positive constant delays $\{\tau_1, \tau_2, \ldots, \tau_{n_\tau}\}$, and the continuously differentiable function $g : \mathbb{R}^n \times \mathbb{R}^n \times \cdots \times \mathbb{R}^n \to \mathbb{R}^n$. Eq. (1) characterizes many physical systems with more than one delay. Some examples of systems with multiple delays in-

* Corresponding author.
E-mail address: firas.khasawneh@duke.edu (F.A. Khasawneh).

1007-5704/$ - see front matter © 2012 Elsevier B.V. All rights reserved.
http://dx.doi.org/10.1016/j.cnsns.2012.11.030

clude traffic stability models [12–15], laser systems [2,16] and variable pitch mills [17,18]. The existence of multiple delays in the system often leads to complicated stability structures in the delays parameter space. Specifically, increasing one of the delays may stabilize the system whereas increasing one of the other delays can destabilize the same system.

The stability of equilibria for Eq. (1) is determined by its linearized variational form given by

$$\frac{dx}{dt} = A(t)x(t) + \sum_{k=1}^{n_\tau} B_k(t)x(t-\tau_k), \tag{2}$$

where the $n \times n$ system matrices in Eq. (2) are given by

$$A(t) = \frac{\partial}{\partial \zeta_0} g(\zeta_0, \zeta_1, \ldots, \zeta_{n_\tau}), \tag{3a}$$

$$B_k(t) = \frac{\partial}{\partial \zeta_k} g(\zeta_0, \zeta_1, \ldots, \zeta_k, \ldots, \zeta_{n_\tau}). \tag{3b}$$

In this study, we consider the autonomous ($A(t) = A, B_k(t) = B_k$) case and the non-autonomous time-periodic case ($A(t+T) = A(t), B_k(t+T) = B_k(t)$) and examine the stability of stationary solutions and periodic orbits of Eq. (1), respectively. We make no assumptions on the ratio between the delay τ and the period T or on the number of delays τ_k. This introduces more challenges to the analysis due to the multiple time delays and the decoupling of the delay and the period.

The difficulties associated with studying multiple time delay systems MTDS is evidenced by the limited literature on the topic. For example, time integration methods were developed based on either discretizing the solution operator [19–21] or discretizing the infinitesimal generator of the solution operator semigroup [22,23]. Analytical methods have also been used to study the stability of MTDS. For instance, Hale and Huang studied the stability of autonomous first order MTDS [24] using D-subdivision. Stepan [25] and Niculescu [26] investigated autonomous second order MTDS using D-subdivision and a frequency domain approach, respectively, but without damping terms. Sipahi and Olgac used the Cluster Treatment of Characteristic Roots method to study the stability of autonomous second order MTDS including damping [27]. The stability of autonomous MTDS was also studied in Ref. [28] using the Continuous Time Approximation method (CTA). However, the CTA method often results in very large matrices which can lead to computational difficulties.

Moreover, decoupling the delay and the period and allowing them to vary independently introduces an additional time scale into the DDE. This scenario arises, for example, in the study of periodic solutions of nonlinear DDEs. The competition between the two time scales T and τ influences the value of the largest eigenvalue which leads to drastic changes in the stability boundaries [29]. In order to study a DDE with decoupled T and τ, it is necessary to construct the correct mapping for each combination of T and τ.

The different mappings associated with different T to τ ratios are shown in Fig. 1(b)–(d). In these figures, the history segments, denoted by the light gray lines, are mapped ahead by one period onto the interval marked by the dark gray lines. Graph (a) shows the mapping of an ODE ($\tau = 0$) with T-periodic coefficients—where τ here denotes the maximum delay. For this case, Floquet theory states that it is sufficient to map the states at any instant one period ahead to create a dynamic map and investigate the system stability. However, for $\tau \neq 0$, i.e. Fig. 1(c) and (d), it is necessary to map the states described by the history function one period ahead.

Since it is often impossible to deal directly with the infinite dimensional DDE, it must first be discretized to produce a finite dimensional approximation. The idea is that as the degree of approximation increases, the solution of the finite dimensional problem converges to that of the infinite dimensional problem. The goal of the approximation is to construct a finite dimensional dynamic map in the form

$$x_m = U x_{m-1}, \tag{4}$$

where x_m and x_{m-1} are the vectors of the discretized states on $[0, T]$ and $[-\tau, T-\tau]$, respectively, whereas U is the monodromy matrix, which represents a finite dimensional approximation to the infinite dimensional monodromy operator. The monodromy operator U corresponds to the evolution family E of the linearized system (a two-parameters semigroup, see e.g. Ref.

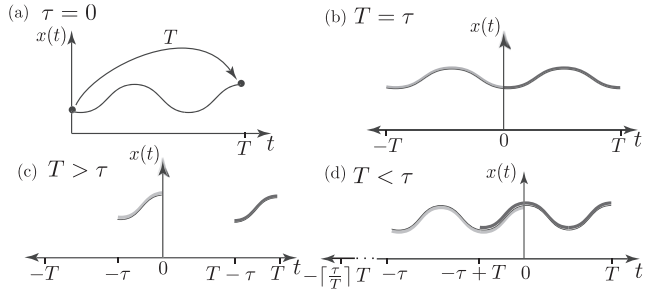

Fig. 1. The different mappings necessary to create an approximate monodromy matrix for (a) $\tau = 0$, (b) $T = \tau$, (c) $T > \tau$, and (d) $T < \tau$.

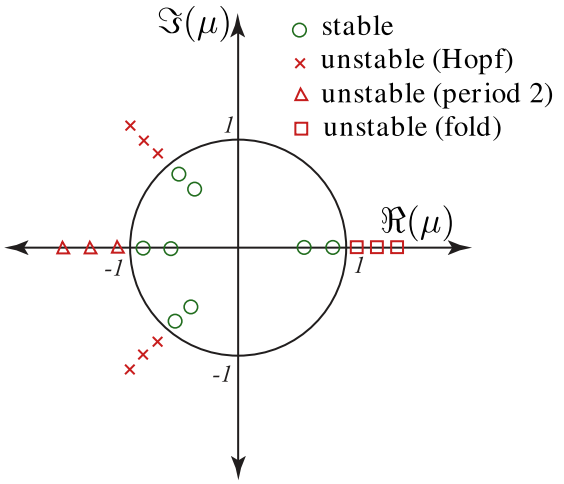

Fig. 2. The stability criteria dictates that all the eigenvalues, μ, of the monodromy operator U, should lie within the unit circle in the complex plane. Moreover, the manner in which the eigenvalues depart the unit circle produces different bifurcation behavior. For example, an eigenvalue leaving the unit circle through -1 or 1 results in a period doubling bifurcation or a fold bifurcation, respectively, whereas two complex conjugate eigenvalues departing the unit circle results in secondary Hopf bifurcation.

[30]) as evaluated in the coefficients' period T with initial instant 0, namely $U = E(T, 0)$. This operator brings the initial state defined on $[-\tau, 0]$, where τ is the maximum delay, into the state after one period T living hence on $[T - \tau, T]$. The stability of the system is then investigated using the eigenvalues of U according to the criteria shown in Fig. 2.

Insperger and Stepan investigated the stability of autonomous as well as non-autonomous second order MTDS using the semi-discretization approach [31]. However, the semi-discretization approach often results in large matrices and long computational times. A collocation method for the stability of MTDS based on piecewise polynomials was analyzed in Refs. [32,33]. However, as was shown in Refs. [34,35], the spectral element method can have higher rates of convergence than collocation methods.

This paper describes a general spectral element approach to study the stability of multiple time delay systems (MTDS). We show, for the first time, how this approach can be applied to periodic MTDS where the delays and the period are incommensurate. In contrast to prior works on MTDS, the spectral element approach is applicable to both autonomous as well as non-autonomous MTDS. Both MTDS of first order or higher can be obtained and systems with or without damping can be investigated. Since the spectral element approach uses efficient interpolation and a set of well-distributed interpolation points, the size of the matrices necessary for convergence is kept small. Further, since the spectral element approach is a semi-analytical procedure, it avoids the need to use tedious time marching algorithms to explore the stability behavior of the system.

This paper is organized into two main parts. The first part (Sections 2–4) describes the generalization of the spectral element method to single-delayed time-periodic DDEs with general T to τ ratios. The second part (Sections 5 and 6) further generalizes the spectral element method to time-periodic DDEs with multiple delays. The specific breakdown of the sections is as follows. Section 2 describes the spectral element approach for the stability analysis of delays systems. Section 3 describes the matrix structures associated with constructing a dynamic map for DDEs with different T to τ ratios. Case studies for the different delay and period ratios are presented in Section 4. Section 5 extends the approach to the multiple delays case. Section 6 shows several case studies of MTDS and the paper ends with the conclusions in Section 7.

2. Spectral element method

The stability of DDEs can be studied using the spectral element approach. To elaborate consider the general DDE described by

$$\dot{x} = f(x(t), x(t-\tau), t) \quad \text{for } t \in [0, T], \tag{5a}$$

$$x(t) = \varphi(t) \quad \text{for } t \in [-\tau, 0], \tag{5b}$$

where $x \in \mathbb{R}^n$, f is smooth, T is the system period while the scalar τ is a positive time delay. The function φ describes the history segment for $t \in [-\tau, 0]$. Note that for autonomous systems T is not unique and can be chosen arbitrarily; however, for convenience, it is usually chosen as $T = \tau$.

The first step is to discretize the period $[0, T]$ using a finite number of temporal elements E. Each element is described by the interval

$$e_j = [t_j^-, t_j^+), \tag{6}$$

where t_j^- and t_j^+ denote the left and right element boundaries, respectively, with the length of the jth element given by

$$h_j = t_j^+ - t_j^-. \tag{7}$$

Within each element, a local normalized time $\eta = \sigma/h_j$ is defined where $\sigma \in [0, h_j]$ is the local time while $\eta \in [0, 1]$. The barycentric Lagrange formula is then used to obtain an approximate expression for the states over each element using a set of local interpolation nodes normalized by h_j. For example, if $n+1$ interpolation nodes were used then the approximate states over the jth element are given according to

$$x_j(t) = \sum_{i=1}^{n+1} \phi_i(\eta) x_{ji}, \tag{8}$$

where $x_{ji} = x_j(t_i)$ with i indicating the ith interpolation node within the element and ϕ_i are the trial functions that can be calculated using the barycentric Lagrange formula according to [36]

$$\phi_i(\eta) = \frac{\frac{\varpi_i}{\eta - \eta_i}}{\sum_{k=1}^{n+1} \frac{\varpi_k}{\eta - \eta_k}}, \tag{9}$$

where for node η_k the trial functions must satisfy

$$\phi_i(\eta_k) = \begin{cases} 1, & i = k, \\ 0, & i \neq k, \end{cases} \tag{10}$$

while ϖ_k are the barycentric weights given by

$$\varpi_k = \frac{1}{\prod_{k \neq j}(\eta_j - \eta_k)}, \quad j = 1, \ldots, n+1. \tag{11}$$

In this study we use Eq. (9) to obtain the trial functions since it has better numerical stability and requires less computation than the conventional Lagrange representation [37,36]. In addition to being a more efficient tool to generate the trial functions, the barycentric weights can be used to obtain the value of the derivative of the trial functions evaluated at the interpolation nodes according to

$$\phi_i'(\eta_k) = \begin{cases} \frac{\varpi_i/\varpi_k}{\eta_i - \eta_k}, & i \neq k, \\ \sum_{i=0, i\neq k}^{n+1} \frac{-\varpi_i/\varpi_k}{\eta_i - \eta_k}, & i = k. \end{cases} \tag{12}$$

Substituting the expression from Eq. (7) into Eq. (5) gives

$$\sum_{i=1}^{n+1} \frac{1}{h_j} \dot{\phi}_i(\eta) x_{ji} - f\left(\sum_{i=1}^{n+1} \phi_i(\eta) x_{ji}, \sum_{i=1}^{n+1} \phi_i(\eta^*) x^q_{j^*(t^*),i}, t_j^- + \eta h_j \right) = \text{error}, \tag{13}$$

where the residual error is due to the approximation procedure while the time t^* is defined using modular arithmetics according to

$$t^* = t_j^- + \eta h_j - \tau (\text{mod} T). \tag{14}$$

Eq. (14) is used to define the local normalized time according to

$$\eta^* = \frac{t^* - t_j^{*-}}{h_j^*}, \tag{15}$$

where t_j^{*-} is the left boundary of element $j^* = j^*(t^*)$ while h_j^* is its length. The function $j^*(t^*)$ gives the element index to which t^* belongs which (for uniformly distributed elements) is given by

$$j^*(t^*) = \left\lceil \frac{t^*}{h} \right\rceil, \tag{16}$$

where $\lceil \cdot \rceil$ is the ceiling function and h is the length of each of the uniform elements.

The integer q in Eq. (13) is the number of the period to which the delay looks back and it is described by

$$q = \left| \left\lfloor \frac{t - \tau}{T} \right\rfloor \right|, \tag{17}$$

where $\lfloor \cdot \rfloor$ is the floor function and with the understanding that $q = 0$ indicates a mapping onto the interval $[0, T]$.

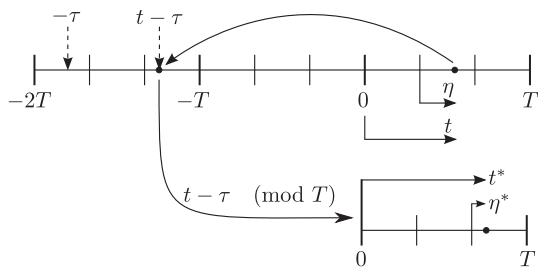

Fig. 3. Illustration showing the steps necessary to construct a dynamic map for DDES with arbitrary T and τ ratios.

As an example, consider the mapping shown in Fig. 3. In this figure, 3 elements were used to discretize the interval $[0,T]$ and the delay was assumed to map back to at most 2 periods in the past. Note that the same discretization needs to be used in all previous periods affected by the delay term.

Fig. 3 shows the mapping of an arbitrary node $\eta \in \{\eta_i\}_{i=1}^{n+1}$ in the second element at time $t \in [0,T]$ (Without making any assumptions on the number of interpolation points used within each element). The node is mapped onto a point in the interval $[-2T,-T]$. Since the whole time-line is discretized using the same mesh in each interval of length T, Eq. (14) and (16) can be used to find the element j^* where the point will map to ($j^*=3$ in this example). The local time within that element can be found using Eq. (15) and, in general, it will not align with one of the interpolation nodes within that element. When the mapped points align with the mesh points, the mesh is called a constrained mesh, otherwise it is called an unconstrained mesh [38].

When dealing with unconstrained meshes, interpolation becomes necessary because the mapped states do not align with the discretization mesh. The interpolation describes the states at t^* in terms of the states at the interpolation nodes in the j^*th element within the qth period using Eqs. (8) and (19). Specifically, this interpolation can be described using an interpolation matrix according to

$$x(\eta^*) = \Upsilon_{(\eta^*\to\eta)} x_{j^*}^q, \tag{18}$$

where Υ is the interpolation matrix from η^* onto $\{\eta_i\}_{i=1}^{n+1}$ while $x_{j^*}^q$ is the vector of states in the j^* element within the previous qth period ($q=2$ in Fig. 3). To elucidate the role of the interpolation matrix, define a vector of base points $x_1 \in \mathbb{R}^{n\times 1}$, and let a vector of arbitrary albeit unique points be $x_2 \in \mathbb{R}^{m\times 1}$, then the effect of interpolating x_2 using x_1 as the base points is described using the linear transformation

$$x_2 = \Upsilon x_1, \tag{19}$$

where $\Upsilon \in \mathbb{R}^{m\times n}$ is called the interpolation matrix. The entries of the interpolation matrix are calculated using Eq. (9) according to

$$\Upsilon_{ji} = \phi_i(\eta_j), \tag{20}$$

where $\eta_j \in x_2$ and $i \in 1,2,\ldots,n+1$. Eqs. (19) and (20) define a linear transformation useful in mapping unconstrained meshes and multiple time delays as will be shown in the subsequent sections.

We use the method of weighted residual to minimize the approximation error in Eq. (13) [39]. Specifically, Eq. (13) is multiplied by a set of independent weight functions $\psi_p(\eta)$ where $p=1,2,\ldots,n$ and is integrated over the normalized length of each element according to

$$\int_0^1 \left[\sum_{i=1}^{n+1}\frac{1}{h_j}\dot{\phi}_i(\eta)x_{ji} - f\left(\sum_{i=1}^{n+1}\phi_i(\eta)x_{ji}, \sum_{i=1}^{n+1}\phi_i(\eta^*)x^q_{j^*(t^*),i}, t_j^- + \eta h_j\right)\right]\psi_p(\eta)\,d\eta = 0. \tag{21}$$

In this study we chose the weight functions to be the set of the n shifted Legendre polynomials. The weighted residual integral in Eq. (21) is often difficult to evaluate analytically. Therefore, analytical integration is substituted by a quadrature rule which uses $m+1$ quadrature points over each element according to

$$\sum_{k=1}^{m+1} w_k\left[\sum_{i=1}^{n+1}\frac{1}{h_j}\dot{\phi}_i(\eta_k)x_{ji} - f\left(\sum_{i=1}^{n+1}\phi_i(\eta_k)x_{ji}, \sum_{i=1}^{n+1}\phi_i(\eta_k^*)x^q_{j^*(t^*),i}, t_j^- + \eta_k h_j\right)\right]\psi_p(\eta_k) = 0, \tag{22}$$

where $\{\eta_k\}_{k=1}^{m+1}$ and w_k are the quadrature nodes and weights, respectively. If we choose the quadrature nodes to coincide with the LGL interpolation nodes—i.e., $\{\eta_k\}_{k=1}^{m+1} = \{\eta_k\}_{i=1}^{n+1}$—we can define a highly accurate Gaussian quadrature. Further, forcing the quadrature nodes to align with the mesh points allows using Eq. (10) to further simplify Eq. (21).

To construct a dynamic map, each discretization point in $[0,T]$ is mapped by τ. Eq. (18) needs to be used whenever interpolation is needed. Since f is linear in x_{ji} and $x^{q_k}_{j^*(t_k^*),i}$, applying Eq. (22) to all the elements using the n weight functions yields a

set of $d \times n$ algebraic equations (d is the order of the DDE). In addition, enforcing the continuity condition at $t = 0$ gives d additional equations for a total of $d(n+1)$ equations.

The coefficients of the discretized states in the interval $[0, T]$ can be arranged into a matrix H while the coefficients of the discretized states in the interval $[-\lceil \frac{\tau}{T} \rceil T, 0]$ can be assembled into a second matrix G. Consequently, the mapping from the states $x_m \in [0, T]$ onto $x_{m-1} \in [-\lceil \frac{\tau}{T} \rceil T, 0]$ is described by the dynamic map

$$x_m = H^{-1} G x_{m-1} = U x_{m-1}, \tag{23}$$

where $U = H^{-1}G$ is the monodromy matrix described in Eq. (4). Alternatively, the inversion of H can be avoided by solving the generalized eigenvalue problem $|G - \mu H| = 0$ for the eigenvalues μ. The stability of Eq. (5) is then ascertained by examining the eigenvalues μ (or characteristic multipliers) of U: the system is stable if all the eigenvalues are within the unit circle in the complex plane, as shown in Fig. 2.

3. Mapping considerations

The size and the structure of H and G depend on the mesh and on the ratio between T and τ. The following sections describe more details about the mapping associated with each T to τ ratio and provide comments on the resulting matrix structures.

3.1. Case 1 : $\tau = T$

The case of autonomous DDEs or of DDEs with $T = \tau$ is shown in Fig. 1(b). This case results in a constrained mesh where each point is mapped exactly onto a corresponding discretization point. A mesh with this property is called a constrained mesh and if it is combined with an appropriate choice of discretization points, such as Legendre–Gauss points, it gives rise to fast convergence as the number of points is increased (called super-convergence, see Ref. [32]). In contrast, the case $T \neq \tau$ gives rise to an unconstrained mesh and necessitates the use of an interpolation matrix (see Eq. (19)). Specifically, let the order of the DDE be d, the size of the discretization mesh be $n+1$ and the number of elements E; then the resulting matrices have the same size which is equal to $d(En+1) \times d(En+1)$.

Consider for example the state-space discretization shown in Fig. 4a for a DDE with $\tau = T$. The goal here is to approximate the monodromy matrix by constructing a map between the delayed states denoted by the blue 'X' and the states one period ahead, denoted by the green 'O'. Notice that the interval $[0, T]$ was discretized using 3 elements and 5 interpolation nodes within each element. To describe mapping the states, consider the 3rd node within the 5th element. The local time for this node is η_3 while the global time is t_7 since globally this is the 7th node. Since $T = \tau$, due to the delay τ this node will look back at a corresponding node in the previous period and the local time for that delayed node will also be η_3. Therefore, for the case $T = \tau$ no interpolation is necessary since the delayed states always line up with a mesh point. Mapping all the discretized states in $[0, T]$ is done in a similar fashion. The equations describing the map can be arranged into a matrix equation; all the coefficients multiplying the states on $[0, T]$ are arranged into a matrix H whereas the coefficients multiplying the states on $[-\tau, T]$ are arranged into another matrix G.

Using the example discretization in Fig. 4(a) and assuming the DDE is of first order, then the sizes of the resulting H and G matrices are shown in Fig. 4(b). Recall that the stability is determined by the eigenvalues of the monodromy matrix $U = H^{-1}G$ as was described in Section 2. Note that for this case the entries are block matrices aligned in a band near the diagonal and all the entries off this band are zeros except the last d rows. These last d rows in both the H and the G matrix contain the $d \times d$ identity matrix multiplying the point $x(0)$ to enforce the continuity condition at $t = 0$.

However, when $T \neq \tau$, it is necessary to interpolate using Eq. (19) since, in general, the mesh points do not map exactly onto the corresponding mesh points as will be shown in the following sections.

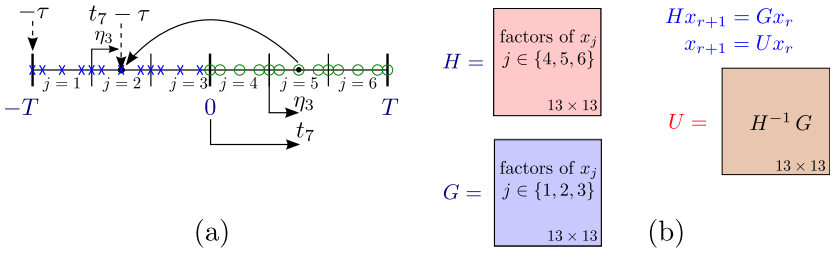

Fig. 4. Example discretization of the state-space over the period T when $\tau = T$. (a) Shows the discretization of the time-line over each T using 3 temporal elements with 5 nodes within each element. (b) Describes the sizes of the resulting map matrices H, G, and U when the DDE is assumed to be of first order.

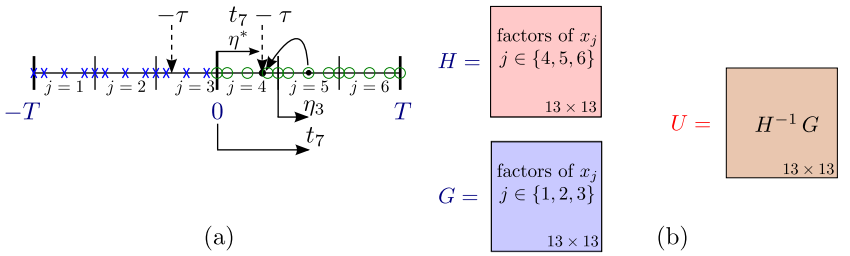

Fig. 5. Example discretization of the state-space over the period T when $\tau < T$. (a) Shows the discretization of the time-line over each T using 3 temporal elements with 5 nodes within each element. (b) Describes the sizes of the resulting map matrices H, G, and U when the DDE is assumed to be of first order.

3.2. Case 2 : $\tau < T$

The case $T > \tau$ is shown in Fig. 1(c). Whereas for $t < 0$ the history function gives the values of the states, the evolution for $t \geqslant 0$ is governed by the DDE. To obtain the correct mapping for this case, the period $[0, T]$ is discretized and the DDE is used to obtain the mapping from $[-T, 0]$ onto $[0, T]$. Interpolation should be used whenever the mesh points do not line up in the two intervals (see Eq. (19)) while the last d rows are modified to enforce the continuity condition at $t = 0$. The sizes of the resulting matrices are similar to the case $T = \tau$ as shown in Fig. 5(b) which describes the H and G matrices for a first order DDE. However, the structures of the H and the G matrices are different. Specifically, since the T and τ ratio can cause interim mapping as shown in Fig. 5, the delay term modifies some terms in the H matrix in addition to modifying the G matrix.

To elaborate, consider the sample discretization shown in Fig. 5(a) where the 3rd node within the 5th element is being mapped by τ. For a general τ and T ratio, τ maps that node into an interim region which for this example lies in the 4th element between the 3rd and 5th local nodes. The local time at the delayed state is η^* and the states at that node can be approximated using the states within the 4th element using Eq. (19). Similarly, each mesh point is mapped to construct the monodromy matrix as shown in Eq. (23). The stability can then be ascertained by examining the eigenvalues of the resulting monodromy matrix.

3.3. Case 3 : $\tau > T$

Fig. 1(d) shows the case $T < \tau$ where two differences in comparison to the prior cases can be observed: (1) the delay term looks back more than one period up to $N_T = \lceil \tau/T \rceil$ periods where $\lceil \cdot \rceil$ denotes the ceiling function, and (2) mapping the history function one period ahead results in an interval where the history function and the mapped states overlap.

A consequence of (1) is that the G matrix in Eq. (4) needs to be extended to cover the maximum number of periods the delay looks back. To illustrate, consider Fig. 6(a) which shows a discretization of each period T using 3 elements and 5 interpolation points. If we focus on the 3rd local node within the 8th element, we see that the delayed states at this point lie within the 3rd element in $[-2T, -T]$. The local time at the delayed states is η^* and it can be used to interpolate the delayed states

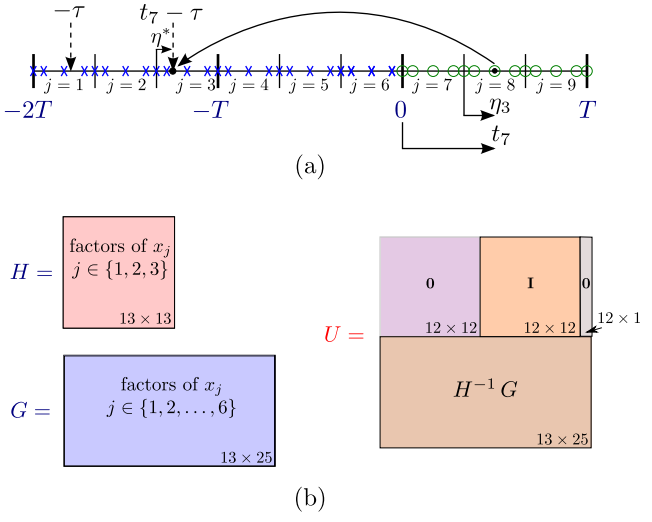

Fig. 6. Example discretization of the state-space over the period T when $\tau > T$. (a) Shows the discretization of the time-line over each T using 3 temporal elements with 5 nodes within each element. (b) Describes the sizes of the resulting map matrices H, G, and U when the DDE is assumed to be of first order.

in terms of the discretized states within the 3rd element using Eq. (19). If the discretization in Fig. 6(a) is for a 1st order DDE, then the resulting structure of the H and G matrices is shown in Fig. 6(b). Fig. 6(b) shows how the G matrix is extended to cover the maximum number of periods the delay looks back. For this specific example $N_T = 2$ and for $t > 0$ the delayed term acts on the period $[-2T, -T]$.

Generally, if the period T is discretized using E elements with $n+1$ local interpolation points, then a DDE of order d results in an H matrix of size $d(En+1) \times d(En+1)$—similar to the above two cases—whereas the size of the G matrix is $d(En+1) \times d(N_T En+1)$. The delay and period can be either commensurate or incommensurate.

The forms of H and G described above constitute the contribution from the evolution of the DDE. To account for the overlap shown in Fig. 1(d), and described in point (2) above, additional equations need to be added to the monodromy matrix. Specifically, the monodromy matrix takes the form

$$U = \begin{bmatrix} 0_{(d(N_T-1)En)\times dEn} & I_{d(N_T-1)En} & 0_{(d(N_T-1)En)\times d} \\ & H^{-1}G & \end{bmatrix}, \tag{24}$$

where I is an identity matrix and 0 is a matrix of zeros. The eigenvalues of U can then be used to determine the stability of the DDE according to the criteria shown in Fig. 2. The structure of U is shown pictorially in Fig. 6(b).

4. Examples on different T and τ ratios

The complication of different ratios of T to τ is investigated using the delayed damped Mathieu equation [40]

$$\ddot{x}(t) + \kappa\dot{x}(t) + (\delta + \epsilon\cos(2\pi/T))x(t) = bx(t-\tau), \tag{25}$$

where ϵ and δ are scalars, the time period is T, and the constant positive delay is τ.

Fig. 7 shows the stability diagrams for Eq. (25) corresponding to different combinations of T and τ as well as different values for κ and ϵ. The first column corresponds to $\epsilon = 1$ whereas the second row corresponds to $\epsilon = 2$. The results in Fig. 7 are in agreement with the results obtained in Ref. [40] using the semi-discretization method. Fig. 7(a) and (b) show the stability diagram for the case $T = \tau/2 = \pi$ which was obtained using $E = 2$ and $n = 5$. This case corresponds to Section 3.2 where the case $T < \tau$ was described. However, note that since the delay and the period are commensurate, a constrained mesh is the natural choice. Figs. 7(c) and (d) show the stability diagram for the case $T = \tau/\sqrt{2} = \sqrt{2}\pi$ which was obtained using $E = 2$ and $n = 10$. This case also corresponds to Section 3.2; however, in contrast to Fig. 7(a) and (b), this case represents incommensurate period and delay resulting in unconstrained meshes.

The stability chart for the case $T = \tau = 2\pi$ is shown in Figs. e,f where the parameters $E = 2$ and $n = 5$ were used. This case corresponds to the case described in Section 3.1. The case $T = \sqrt{2}\pi$ is shown in Figs. 7(g) and (h). This case corresponds to Section 3.2 where $T > \tau$. Note that the resulting mesh is unconstrained since the ratio between the delay and the period is incommensurate. The parameters $E = 2$ and $n = 5$ were used to produce Fig. 7(g) and (h). Finally, the case $T = 2\tau = 4\pi$ is shown in Fig. 7(i) and (j). This case also corresponds to Section 3.2 where the inequality $T > \tau$ is true. However, in contrast to Fig. 7(g) and (h), the ratio between T and τ is commensurate and the mesh can be chosen to be constrained.

5. Multiple delays

The spectral element approach can also be extended for multiple time delay systems (MTDS) both with autonomous and time-periodic coefficients. No assumptions are made on the ratio between any of the delays and the period. Section 5.1 describes the generalization of the spectral element approach to MTDS. The effectiveness of the developed approach is demonstrated in Section 6 using a set of case studies. Specifically, Section 6.1 investigates the stability of a scalar MTDS [24,41]. Section 6.2 studies the stability of a second order MTDS with cross talking delays [27] while Section 6.3 investigates the stability of a second order MTDS with time-periodic coefficients.

5.1. Analysis of MTDS using spectral element approach

Differential equations with multiple discrete delays can be described by

$$\dot{x}(t) = f\left(x(t), \sum_{k=1}^{n_\tau} x(t-\tau_k)\right), \tag{26}$$

where $x \in \mathbb{R}^n$, n_τ is the number of delays and f is smooth and is linear in x.

To perform the stability analysis of Eq. (26) using the spectral elements method, the interval $[0, T]$ is discretized for each period T into a set of temporal elements. If the MTDS is autonomous, then T is set to $\max_{1\leqslant k\leqslant n_\tau}(\tau_k)$ merely for convenience. Within each element, an approximate solution is defined on a set well-distributed nodes according to Eq. (8). Substituting the expression for the approximate states over the jth element into Eq. (26) yields

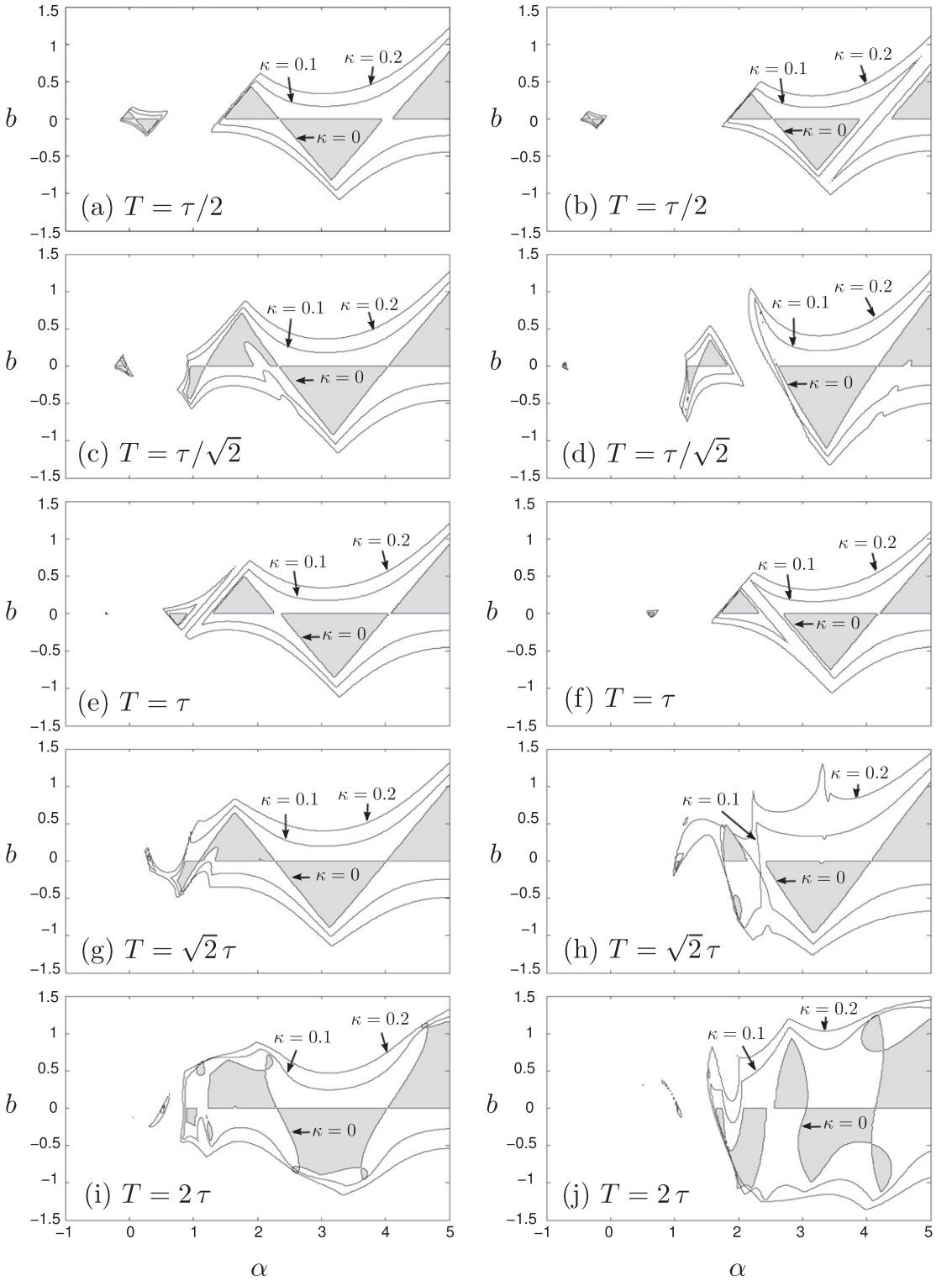

Fig. 7. The stability diagrams of Eq. (25) using different T to τ ratios and various values for κ and ϵ (200×200 grid). The first and second columns correspond to $\epsilon = 1$ and $\epsilon = 2$, respectively. $E = 2,\ n = 5$ in (a)–(f) whereas $E = 2,\ n = 10$ in (g)–(j).

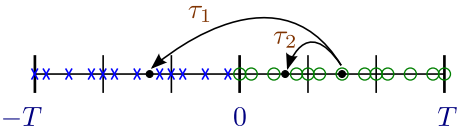

Fig. 8. The mapping of the states for an MTDS with $\max(\tau_1, \tau_2) < T$ at a mesh node by two delays τ_1 and τ_2.

$$\sum_{i=1}^{n+1} \dot{\phi}_i(\eta) x_{ji} - f\left(\sum_{i=1}^{n+1} \phi_i(\eta) x_{ji}, \sum_{k=1}^{n_\tau} \sum_{i=1}^{n+1} \phi_i(\eta_k^*) x^q_{j^*(t_k^*),i} \right) = \text{error}, \tag{27}$$

where the residual error is due to the approximation procedure while h_j is the length of the jth element, see Section 2. The time t_k^* is defined using modular arithmetics according to

$$t_k^* = t_j^- + \eta h_j - \tau_k (\text{mod} T), \tag{28}$$

where t_j^- is the left boundary of the jth element. Eq. (28) is used to define the local normalized time according to

$$\eta_k^* = \frac{t_k^* - t_j^{*-}}{h_j^*}, \tag{29}$$

where t_j^{*-} is the left boundary of the element $j^* = j^*(t_k^*)$ while h_j^* is its length. the function $j^*(t_k^*)$ gives the element index to which t_k^* belongs and it is obtained by making the substitution $t^* = t_k^*$ in Eq. (16).

The integer q_k in Eq. (27) is the number of the period to which the delay looks back and it is described by

$$q_k = \left| \left\lfloor \frac{t - \tau_k}{T} \right\rfloor \right|, \tag{30}$$

where $\lfloor \cdot \rfloor$ is the floor function and with the understanding that $q_k = 0$ indicates a mapping onto the interval $[0, T]$.

The method of weighted residuals described in Section 2 can then be used to reduce the approximation error and create a dynamic map over one period for Eq. (26). Note that since there is more than one delay, the discretized states at each point are mapped back by each τ_k. The mapping is different for the different types of MTDS. Specifically, whereas it is usually convenient to choose $T = \max_{1 \leqslant k \leqslant n_\tau}(\tau_k)$ for autonomous systems, mapping non-autonomous systems depends on the ratio between the maximum delay $\tau_{\max}$ and the period T. For example, Fig. 8 shows how two delays τ_1 and τ_2 map the same states back to different elements for a DDE with $\tau_{\max} = T$. For the cases $\tau < T$ or $\tau > T$, interpolation is necessary whenever the mapped nodes in $[0, T]$ do not line up with any of the prior nodes, see Section 3. The eigenvalues of the map can be used to ascertain the system stability using the criteria in Fig. 2.

6. MTDS case studies

This section uses 3 case studies to demonstrate the effectiveness of the stability analysis using spectral element approach. Section 6.1 studies an introductory scalar MTDS. Section 6.2 investigates the stability of a 2nd order MTDS with a cross-talk delay term, i.e. one of the delays is a combination of the other delays. Section 6.3 studies a 2nd order MTDS with time-periodic coefficients.

6.1. Scalar MTDS

Consider the scalar MTDS

$$\dot{x}(t) + x(t) + 2x(t - \tau_1) + 2x(t - \tau_2) = 0. \tag{31}$$

The stable regions for this equation, in the (τ_1, τ_2) space, were studied in Ref. [24] using D-subdivision and in Ref. [41] using the method of Cluster Treatments for Characteristic Roots. Note that the system is autonomous; therefore, we can choose to discretize the period $[0, \max(\tau_1, \tau_2)]$, i.e. choose $T = \max(\tau_1, \tau_2)$. Also note that since the coefficients of the delayed term are equal, it is sufficient to obtain the stability boundaries only below (or above) the line $\tau_1 = \tau_2$ then mirror the boundaries with respect to that line to obtain the full stability diagram. The stability diagram obtained using the spectral element method is shown in Fig. 9(a). This diagram was obtained using $n = 10,\ E = 3$ and a 150×150 grid and it is in agreement with Refs. [24,41].

6.2. Second order MTDS with cross talking delays

Consider the second order MTDS

$$\ddot{x}(t) + 7.1\dot{x}(t) + 21.1425x(t) + 6\dot{x}(t - \tau_1) + 14.8x(t - \tau_1) + 2\dot{x}(t - \tau_2) + 8x(t - \tau_1 - \tau_2) = 0, \tag{32}$$

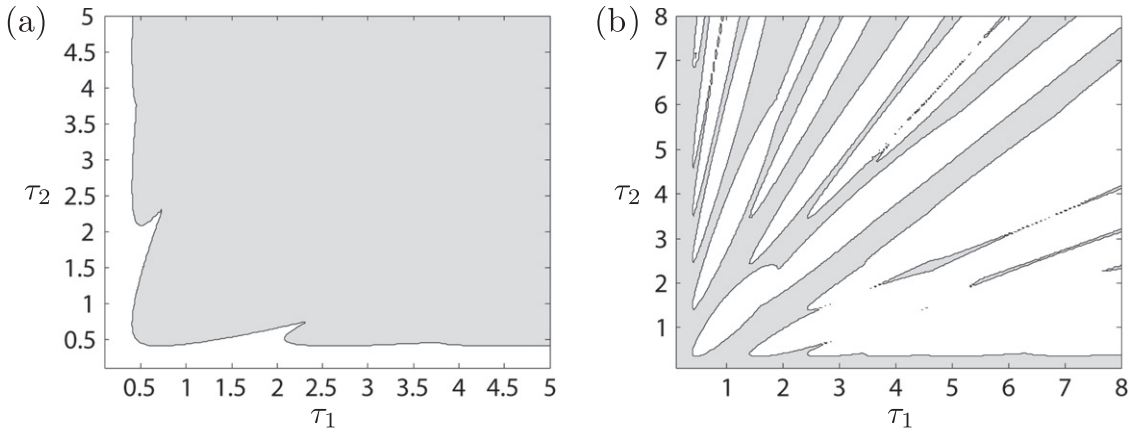

Fig. 9. The stability diagram obtained using the spectral element method for (a) Eq. (31) and (b) Eq. (32), (a) was obtained using $n = 10,\ E = 3$ and 150×150 grid whereas (b) was obtained using $n = 15,\ E = 1$ and 200×200 grid.

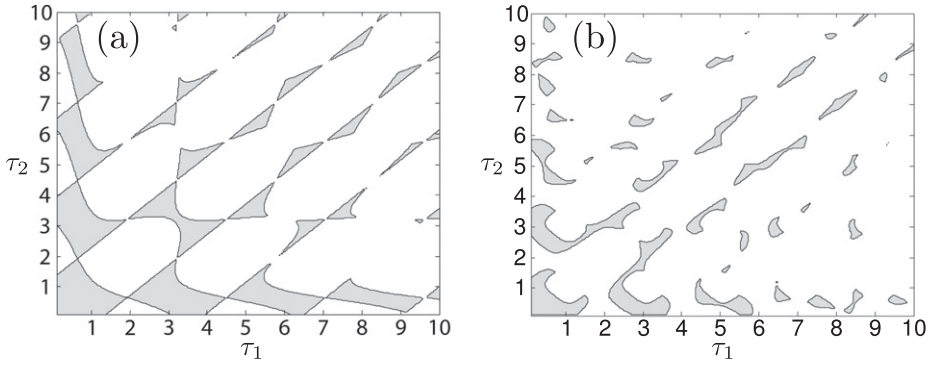

Fig. 10. The stability diagrams corresponding to Eq. (33) using (a) $\epsilon = 0$ and (b) $\epsilon = 6$, (a) was obtained using $n = 15$ and $E = 1$ whereas figure (b) was obtained using $n = 30$ and $E = 1$. Both figures were obtained using point-by-point evaluation on a 200×200 mesh.

where τ_1 and τ_2 are constant positive delays [27]. Note that the last term in Eq. (32) contains the delay cross-talk component. The stability of this system was investigated in Ref. [27] using the Cluster Treatment of Characteristic Roots method (CTCR). Note that since the system is autonomous, it is convenient to choose $T = \tau_1 + \tau_2$ so that the cross talk term will map exactly onto the mesh points whereas interpolation is necessary, in general, for the delays τ_1 and τ_2. The spectral element approach was used to produce the stability diagram for Eq. (32) shown in Fig. 9(b). This diagram is in agreement with Ref. [27] where the CTCR approach was used to obtain the same stability diagram.

6.3. Second order time-periodic MTDS

Whereas Sections 6.1 and 6.2 studied the stability of an autonomous MTDS, this section studies the stability of a 2nd order MTDS with a time-periodic coefficient

$$\ddot{z}(t) + (6 + \epsilon\cos(2\pi t))z(t) = z(t-\tau_1) + z(t-\tau_2). \tag{33}$$

The stability of Eq. (33), in the delay parameter space, is determined by the eigenvalues of the monodromy matrix which can be constructed following the steps in Section 5.1.

The spectral element approach was used to produce the stability diagram for Eq. (33) shown in Fig. 10. Fig. 33(a) corresponds to the choice $\epsilon = 0$ in Eq. (33) resulting in a non-autonomous system. For this choice of $\epsilon,\ T = \max(\tau_1, \tau_2)$ was chosen and the steps outlined in Section 5.1 were followed to obtain the stability boundaries. In contrast, choosing $\epsilon \neq 0$, as in Fig. 10(b) where $\epsilon = 6$, fixes T and the different cases for T and τ ratios described in Section 1 need to be observed. The stability diagrams for both cases were in agreement with the semi-discretization results in Ref. [31]. The parameters $n = 15,\ E = 1$ were used to produce Fig. 10(a) whereas $n = 30$ and $E = 1$ were used in Fig. 10(b). Both figures were obtained by discretizing the (τ_1, τ_2) space using a uniform 200×200 mesh.

7. Conclusions

We described a general spectral element approach to study the stability of multiple time delay systems (MTDS). We showed, for the first time, how this approach can be applied to periodic MTDS where the delays and the period are incommensurate. In contrast to prior works on MTDS, the spectral element approach is applicable to both autonomous as well as non-autonomous MTDS. Both MTDS of first order or higher can be obtained and systems with or without damping can be investigated. Since the spectral element approach uses efficient interpolation and a set of well-distributed interpolation points, the size of the matrices necessary for convergence is kept small. Further, since the spectral element approach is a semi-analytical procedure, it avoids the need to use tedious time marching algorithms to explore the stability behavior of the system.

The contributions from this work were twofold: (1) we described a spectral element approach for studying the stability of time-periodic DDEs, where the delay and the period are decoupled, (2) we then extended the developed spectral element approach to study the stability of DDEs with multiple delays. Developing the spectral element approach for general time-periodic DDEs required discretizing the state-space and establishing the correct mapping for each delay τ to period T ratios.

The different types of meshes that arise when discretizing DDEs with periodic coefficients were analyzed and the associating matrix structures were described in Section 3. Although the period and the delay are equal for a large class of DDEs, they are generally decoupled and can vary independently. When the delay and the period are different, the DDE has two competing time scales that influence the system stability.

For example, when the delay and the period are equal, the resulting mesh points are mapped exactly onto previous points and the mesh is called a constrained mesh. Constrained meshes eliminate the need for interpolation and they can lead to high rates of convergence called super-convergence. In contrast, when the delay and period are unequal, the resulting unconstrained mesh generally maps some points onto interim regions in the mesh—necessitating the use of interpolation. Some exceptions include cases where the ratio of τ to T is rational (see for example Fig. 7(a),(b),(i) and (j)). Specifically, choosing the length of the temporal element in these cases to be equal to the length of the smaller time scale can lead to constrained meshes.

To show the effect of different period to delay ratios on stability a set of stability diagrams for the delayed damped Mathieu equation was shown in Fig. 7. Fig. 7(a)–(d) corresponded to the case $T < \tau$ described in Section 3.3. Whereas Fig. 7(a) and (b) described a constrained mesh (T and τ are commensurate), cases c and d corresponded to an unconstrained mesh since T and τ were incommensurate. Fig. 7(e)–(f) corresponded to the case $T = \tau$ which was described in Section 3.1. This case always produces commensurate meshes and the analysis is simplified by having only one time scale in the DDE. On the other hand, Fig. 7(g)–(j) described the case $T > \tau$. Fig. 7(g) and (h) produced unconstrained meshes since the ratio between the period and the delay was irrational. Cases i and j, however, could use a constrained mesh since the ratio between the period and the delay was rational.

The second part of the paper extended the spectral element method to multiple time delay systems. The discretization of the MTDS was shown in Section 5.1 for both the autonomous and the non-autonomous cases. To show the effectiveness of the presented approach, the stability of a set of case studies was investigated.

Specifically, the stability of a scalar MTDS in the delays parameter space was studied in Section 6.1 and the resulting stability diagram was shown in Fig. 9(a). Sections 6.2 and 6.3 investigated the stability of 2nd order MTDS. To elaborate, Section 6.2 studied the stability of a 2nd order autonomous MTDS that included a term with interacting delays while the resulting stability chart was shown in Fig. 9(b). On the other hand, Section 6.3 studied the stability of a 2nd order MTDS with time periodic coefficients while the resulting stability charts were shown in Fig. 10.

For the examples shown in this paper, all the produced stability charts were found to match the results from well-established methods in the literature, namely, D-subdivision, CTCR and semi-discretization. However, in contrast to D-subdivision and CTCR, the presented approach has the advantage of handling time-periodic systems. Moreover, the size of the matrices necessary to ascertain stability were smaller than their semi-discretization counterparts giving the spectral element approach a clear computational advantage.

A note on the convergence of the spectral element approach is in order. General convergence proofs for different discretizations and solution methods are very sparse in the current literature and typically focus on collocation as the solution method, e.g., [33]. In the collocation method, the delay equation is required to hold exactly at finitely many collocation points. The spectral element method described here instead uses weighted integrals across the temporal domain. Nevertheless, there is a connection between collocation methods and the spectral element approach. Specifically, the spectral element and collocation methods differ mainly in the approach they each use to reduce the approximation error and although these two methods may seem different, they are actually closely related [42]. A discussion of the connection between the spectral element approach and collocation methods in Ref. [34] suggest that the former can be thought of as a linear transformation of the latter. Collocation methods are well documented in the literature and a proof of their convergence can be found in Ref. [33]. Since linear transformations are well behaved with respect to continuity and convergence, the spectral element approach preserves the convergence properties of the collocation approach (see Ref. [34] for more details).

References

[1] Tlusty J. Manufacturing processes and equipment. 1st ed. Upper Saddle River, NJ: Prentice Hall; 2000.
[2] Krauskopf B. Unlocking dynamical diversity: optical feedback effects on semiconductor lasers. Bifurcation analysis of lasers with delay. New Jersey: Wiley; 2005. pp. 147–183.

[3] Patel BR, Mann BP, Young KA. Uncharted islands of chatter instability in milling. Int J Mach Tools Manuf 2008;48:124–34.
[4] Rodrigues S, Barton DA, Szalai R, Benjamin O, Richardson M, Terry J. Transitions to spike-wave oscillations and epileptic dynamics in a human cortico-thalamic mean-field model. J Comput Neurosci 2009;27(3):507–26. http://dx.doi.org/10.1007/s10827-009-0166-2.
[5] Sieber J, Krauskopf B. Control based bifurcation analysis for experiments. Nonlinear Dyn 2008;51:365–77. http://dx.doi.org/10.1007/s11071-007-9217-2.
[6] Barton DAW, Burrow SG. Numerical continuation in a physical experiment: investigation of a nonlinear energy harvester. J Comput Nonlinear Dyn 2011;6(1):011010. http://dx.doi.org/10.1115/1.4002380.
[7] Hale JK, Lunel SV. Introduction to functional differential equations. New York: Springer-Verlag; 1993.
[8] Guglielmi N, Hairer E. Implementing Radau IIA methods for stiff delay differential equations. Computing 2001;67(1):1–12.
[9] Bellen A, Zennaro M. Numerical solution of delay differential equations. Oxford University Press; 2003.
[10] Guglielmi N, Hairer E. Users' guide for the code RADAR5 – version 2.1, Tech. rep., Università dell'Aquila, Italy; 2005.
[11] Guglielmi N, Hairer E. Computing breaking points in implicit delay differential equations. Adv Comput Math 2008;29(3):229–47.
[12] Herman R, Montroll E, Potts R, Rothery R. Traffic dynamics: analysis of stability in car following. Oper Res 1959;7:86–106. http://dx.doi.org/10.1287/opre.7.1.86.
[13] Gasser I, Sirito G, Werner B. Bifurcation analysis of a class of 'car following' traffic models. Phys D Nonlinear Phenom 2004;197(3–4):222–41. http://dx.doi.org/10.1016/j.physd.2004.07.008.
[14] Orosz G, Stépán G. Hopf bifurcation calculations in delayed systems with translational symmetry. J Nonlinear Sci 2004;14(6):505–28. http://dx.doi.org/10.1007/s00332-004-0625-4.
[15] Orosz G, Wilson R, Krauskopf B. Global bifurcation investigation of an optimal velocity traffic model with driver reaction time. Phys Rev E 2004;70(2):026207. http://dx.doi.org/10.1103/PhysRevE.70.026207.
[16] Shahverdiev E, Bayramov P, Shore K. Cascaded and adaptive chaos synchronization in multiple time-delay laser systems. Chaos Solitons Fractals 2009;42(1):180–6. http://dx.doi.org/10.1016/j.chaos.2008.11.004.
[17] Olgac N, Sipahi R. Dynamics and stability of variable-pitch milling. J Vib Control 2007;13(7):1031–43. http://dx.doi.org/10.1177/1077546307078754.
[18] Sims ND, Mann B, Huyanan S. Analytical prediction of chatter stability for variable pitch and variable helix milling tools. J Sound Vib 2008;317:664–86.
[19] Engelborghs K, Roose D. Numerical computation of stability and detection of hopf bifurcations of steady state solutions of delay differential equations. Adv Comput Math 1999;10:271–89. http://dx.doi.org/10.1023/A:1018986817622.
[20] Engelborghs K, Roose D. On stability of lms methods and characteristic roots of delay differential equations. SIAM J Numer Anal 2003;40(2):629–50.
[21] Breda D. Solution operator approximations for characteristic roots of delay differential equations. Applied Numerical Mathematics 2006;56(3–4):305–17. http://dx.doi.org/10.1016/j.apnum.2005.04.010. Selected papers, The third international conference on the numerical solutions of volterra and delay equations..
[22] Breda D, Maset S, Vermiglio R. Computing the characteristic roots for delay differential equations. IMA J Numer Anal 2004;24(1):1–19. http://dx.doi.org/10.1093/imanum/24.1.1.
[23] Breda D, Maset S, Vermiglio R. Pseudospectral differencing methods for characteristic roots of delay differential equations. SIAM J Sci Comput 2005;27(2):482–95.
[24] Hale J, Huang W. Global geometry of the stable regions for two delay differential equations. J Math Anal Appl 1993;178:344–62.
[25] Stépán G. Retarded dynamical sytems: stability and characteristic functions. John Wiley & Sons; 1989.
[26] Niculescu S-I. On delay robustness analysis of a simple control algorithm in high-speed networks. Automatica 2002;38(5):885–9. http://dx.doi.org/10.1016/S0005-1098(01)00260-6.
[27] Sipahi R, Olgac N. A unique methodology for the stability robustness of multiple time delay systems. Syst Control Lett 2006;55(10):819–25. http://dx.doi.org/10.1016/j.sysconle.2006.03.010.
[28] Sun J-Q. A method of continuous time approximation of delayed dynamical systems. Commun Nonlinear Sci Numer Simul 2009;14(4):998–1007.
[29] Just W. On the eigenvalue spectrum for time-delayed floquet problems. Phys D Nonlinear Phenom 2000;142(1–2):153–65.
[30] Diekmann O, Gils S, Lunel S, Walther H-O. Delay equations: functional-, complex-, and nonlinear analysis. Springer; 1995.
[31] Insperger T, Stépán G. Semi-discretization method for delayed systems. Int J Numer Methods Eng 2002;55:503–18.
[32] Engelborghs K, Luzyanina T, in 'T Hout KJ, Roose D. Collocation methods for the computation of periodic solutions of delay differential equations. SIAM J Sci Comput 2000;22:1593–609. http://dx.doi.org/10.1137/S1064827599363381.
[33] Engelborghs K, Doedel E. Stability of piecewise polynomial collocation for computing periodic solutions of delay differential equations. Numer Math 2002;91:627–48.
[34] Khasawneh FA, Mann BP. A spectral element approach for the stability of delay systems. Int J Numer Methods Eng 2011;87(6):566–92. http://dx.doi.org/10.1002/nme.3122.
[35] Tweten DJ, Lipp GM, Khasawneh FA, Mann BP. On the comparison of semi-analytical methods for the stability analysis of delay differential equations. J Sound Vib 2012;331(17):4057–71. http://dx.doi.org/10.1016/j.jsv.2012.04.009.
[36] Higham N. The numerical stability of barycentric Lagrange interpolation. IMA J Numer Anal 2004;24(4):547–56. http://dx.doi.org/10.1093/imanum/24.4.547.
[37] Berrut J, Trefethen LN. Barycentric Lagrange interpolation. SIAM Rev 2004;46(3):501–17.
[38] Luzyanina T, Engelborghs K. Computing floquet multipliers for functional differential equations. Int J Bifurcat Chaos 2002;12(12):2977–89.
[39] Reddy J. An introduction to the finite element method. 2nd ed. New York, NY: McGraw-Hill, Inc.; 1993.
[40] Insperger T, Stépán G. Updated semi-discretization method for periodic delay-differential equations with discrete delay. Int J Numer Methods 2004;61:117–41.
[41] Sipahi R, Olgac N, Breda D. Complete stability map of neutral type first order – two time delay systems. In: Proceedings of the 2007 American control conference, marriott marquis hotel at times square, New York City, USA, July 11–13; 2007.
[42] Boyd JP. Chebyshev and Fourier spectral methods. Dover Publications; 2001.